GSA Data Repository 2019342

Bowman, C.N., et al., 2019, Linking the progressive expansion of reducing conditions to a stepwise mass extinction event in the late Silurian oceans: Geology, https://doi.org/10.1130/G46571.1

SUPPLEMENTARY MATERIAL

1. Stratigraphic Correlations and Eustatic Sea Level Change

1.1 Correlation of Gotland and Latvia Localities

The two localities sampled in this study (Fig. 1, DR1), the proximal Gotland locality (Uddvide-1 drill core and related outcrop samples) and the distal Latvia locality (Priekule-20 drill core), have been correlated based on detailed conodont and graptolite biostratigraphy, as well as carbon isotope ($\delta^{13}C_{carb}$) stratigraphy. The graptolite biozones shown in Figures 2 and DR2 were constructed using graptolite data from detailed collections/studies made from the Priekule-20 drill core (e.g., Kaljo et al., 1997; Kiipli et al., 2010). The conodont biozones presented in Figures 3 and DR2 were constructed using conodont data from Jeppsson (2005), which—while not from the Uddvide-1 core—are from nearby sections across southern Gotland within a few kilometers of the sampled drill core. The Gotland outcrop samples used in this study are from the conodont reference sections used by Jeppsson (2005) to establish the global conodont biozonation for this interval of the Ludfordian Stage in the Silurian. Therefore, our geochemical data sets are tied to the biostratigraphy. The Lau conodont extinction is defined by a stepwise series of extinctions beginning within the upper part of the *Polygnathoides siluricus* Biozone (Jeppsson, 2005), and the Kozlowskii graptolite extinction event is defined by the last appearance datum (LAD) of *Neocucullograptus kozlowskii* (Urbanek, 1993; Manda et al., 2012). As neither of our localities contains both conodonts and graptolites, the correlation is reliant on the combined conodont and graptolite biostratigraphic framework from the interbedded

carbonates and graptolitic shales from locations such as the Vidukle drill core, Latvia and the Kosov Quarry and Všeradice sections of the Czech Republic where the Lau CIE has also been documented (Kaljo and Martma, 2006; Lehnert et al., 2007; Manda et al., 2012).

The *Lobograptus scanicus* graptolite Zone, which is a part of the pre-excursion baseline of the distal Latvian locality, was not included in the correlation because it is a Gorstian Stage biozone unlike the rest of the conodont and graptolite biozones that belong to the Ludfordian Stage. The *P. siluricus* conodont Zone correlates with the upper *Saetograptus lientwardinensis*, *Bohemograptus bohemicus tenuis,* and lower *N. kozlowskii* graptolite zones through the pre-excursion baseline and into the rising limb of the Lau CIE (Kaljo and Martma, 2006; Manda et al., 2012; McAdams et al., 2019). The *Icriodontid* conodont Zone correlates to the upper *Bohemograptus bohemicus tenuis* and *N. kozlowskii* graptolite zones that comprise part of the rising limb and into peak values of the Lau CIE (Lehnert et al., 2007; Kozłowski and Sobień, 2012; Manda et al., 2012). The *Icriodontid* Zone is not globally recognized but is an impoverished conodont fauna found during the Lau conodont extinction interval that seems to be unique to Gotland (Jeppsson, 2005; Corradini et al., 2015).

Correlation of peak values through the falling limb of the Lau CIE are based primarily on carbon isotope stratigraphy as there are no graptolites present through a large portion of the Latvia locality, a local expression of the Kozlowskii extinction (e.g., Kaljo et al., 1997). The interval of peak Lau CIE values in the Gotland locality (*Ozarkodina snajdri* conodont Zone) are significantly expanded compared to the Latvian drill core and contain ~30 m of slightly lowered $\delta^{13}C$ values (+3–4‰ vs. +7–8‰) associated with the Burgsvik Sandstone. This change in sedimentary facies has been interpreted to be the result of a prograding delta complex associated with eustatic sea level changes (Eriksson and Calner, 2008; see section 1.2 on sea level below).

The stratigraphic exposures of the Hamra and Sundre formations only record part of the falling limb of the Lau CIE within the upper part of the *O. snajdri* and *Ozarkodina crispa* conodont Zones, and there is no record of the return to baseline values due to the lack of strata on the Island of Gotland. In the Latvian drill core we record the complete falling limb and several meters of post-excursion baseline in the *Monograptus formosus* graptolite Zone. It is likely that the true first appearance datum (FAD) of *M. formosus* is earlier than it is observed in the Latvian drill core in the interval where no graptolites are present. In the most recent Silurian conodont and graptolite biostratigraphic and carbon isotope chemostratigraphic correlations the *M. formosus* graptolite Zone correlates with the upper part of the *O. crispa* conodont Zone (Manda et al., 2012; McAdams et al., 2019).

1.2 Ludfordian Eustatic Sea Level

Reconstructions of sea-level changes are necessary to the understanding of the possible causal mechanisms behind carbon isotope excursions (e.g., Kump et al., 1999; Kozlowski and Munnecke, 2010). From sequence-stratigraphic analysis of multiple cores and outcrops on the island of Gotland, Eriksson and Calner (2008) identified two major sea-level cycles during the Ludfordian Stage. At this proximal setting in the Baltic Basin (Fig. 1), this is seen as two carbonate rimmed shelf sequences during times of higher sea level, with a clastic prograding delta complex deposited during a period of lowered sea level (Eriksson and Calner, 2008; Younes et al., 2017). Despite the progradation of a deltaic environment into this proximal shelf setting being an undoubtedly localized shift in facies, these overall interpretations of sea-level changes in the Baltic Basin are consistent with other eustatic sea-level curves for the late Silurian (Johnson, 2010 and references therein).

As a result of these sea-level changes and sedimentary facies, the $\delta^{13}C_{carb}$ trend from Gotland appears unlike most other Lau CIE records. The Lau CIE on Gotland is documented as a double-peaked event with maximum values of ~+7.5‰ in open marine carbonate facies of the Eke and Burgsvik Oolite (Fig. 3A). However, a negative shift in $\delta^{13}C_{carb}$ values back to ~+3.5‰ corresponds to deltaic facies within the Burgsvik Formation. We attribute the lowered CIE values in the Burgsvik Sandstone Member to a mixed carbon isotope signal of dissolved inorganic carbon from both marine (+7 to +8‰ underlying Eke/overlying Burgsvik oolite) and riverine (~ -7‰; Kump et al., 1999) sources. This trend is not observed in the $\delta^{13}C_{org}$ values, however, and the organic matter is interpreted to be more reflective of global carbon cycle dynamics. This decoupling of $\delta^{13}C$ trends is unlikely to represent diagenesis (see section 3.1 below for further discussion on diagenesis). Additionally, none of the previously published Lau CIE records from other sections within this basin or from other paleocontinents contain this negative shift in the middle of the Lau CIE. We interpret these carbon isotope records as being a product of the local paleoenvironment and unique to the Gotland, Sweden succession.

Deposition of ~30 m of siliclastic dominated Burgsvik Formation has led to a much greater temporal resolution during the positive carbon and sulfur excursions in the Gotland succession, and has resulted in a greater number of isotopic analyses relative to the same interval within the Latvian drill core (Fig. DR2). Where there is a negative shift in the $\delta^{13}C_{carb}$ record, the $\delta^{34}S_{CAS}$ data plateaus with very little isotopic change during the deposition of the Burgsvik Sandstone Member, and subsequently sulfur isotope values continue to rise up-section as carbonate sedimentation resumed. This $\delta^{34}S_{CAS}$ plateau within the Burgsvik Sandstone Member is likely due to a combination of high sedimentation rates keeping up with increased accommodation space locally during the falling stand systems tract (Eriksson and Calner, 2008),

higher temporal data resolution, and the relatively long residence time of sulfate in the ocean. Despite the stratigraphically expanded nature of the shallow shelf Gotland succession, the $\delta^{34}S$ trends still correlate well with that of the deeper shelf Latvian drill core (Fig. 2, 3, DR. 2).

While eustatic sea level did fluctuate during the Ludfordian (e.g. Eriksson and Calner, 2008; Kozłowski and Munnecke, 2010), it is important to note that the major drop in sea level post-dates the geochemical evidence for changes in paleo-redox discussed in the manuscript text. The Lau CIE begins in the lower Eke Formation, prior to the falling stands systems tract and subsequent sea level lowstand that make up the Burgsvik Formation, indicating that the changes in global carbon cycle dynamics occurred before the drop in sea level. The enrichment in Tl isotopes, which indicates the expansion of deoxygenation and coincides with the initial phase of extinctions, even further pre-dates the sea level lowstand. Although weathering of exposed carbonate platforms via sea level drop cannot be completely ruled out during the study interval, these processes were most likely not the primary driver for the Lau CIE.

2. Samples and Methods

Samples were collected from the Priekule-20 drill core, Latvia every ~2 to 4 meters, with finer sampling resolution (every 0.5 to 1.0 meters) that correspond to the Lau carbon isotope excursion (CIE) interval (Kaljo et al., 1997). Samples were collected from the Uddvide-1 drill core, Island of Gotland, Sweden, every ~0.5 to 1 meter, and Gotland outcrop samples collected in ~3-meter intervals stratigraphically above the drill core from outcrops previously studied for conodont biostratigraphy (e.g., Jeppsson, 2005). In each case, intervals with noticeable diagenetic alteration, such as highly recrystallized carbonates, pyritized horizons, and iron oxide staining were avoided while sampling (see discussion Section 3 below on diagenesis). Weathered

edges of outcrop samples and outer margins of drill core samples were mechanically removed via a water-based diamond blade saw. For all procedures other than carbonate carbon isotopes, samples were crushed and then powdered using either an agate mortar and pestle or an alumina ceramic SPEX8510 ShatterBox.

2.1 Carbonate Carbon and Oxygen Isotopes

Between 200 – 500 μg of sample powder for $\delta^{13}C_{carb}$ and $\delta^{18}O_{carb}$ analysis was generated from a micro-drill assembly to avoid obvious secondary minerals for both the Latvia and Sweden study sites. The sample powders were reacted with 4 – 6 drops of 100% H_3PO_4 at 25°C for 24 hours. Stable carbon and oxygen isotope values of the evolved CO_2 gas were then obtained using a ThermoFinnigan Gas Bench II Autocarbonate device coupled to a ThermoFinnigan Delta Plus XP isotope-ratio mass spectrometer (IRMS) at the National High Magnetic Field Laboratory (NHMFL) at Florida State University (FSU). All carbon and oxygen isotope values are reported in standard delta notation (δ) with units in per mil (‰) relative to the Vienna Pee Dee Belemnite (V-PDB) standard. Analytical precision of $\delta^{13}C_{carb}$ and $\delta^{18}O_{carb}$ based on long-term, replicate analysis of NBS-19 and other lab standards are ±0.05‰ and ±0.1‰, respectively.

2.2 Organic Carbon Isotopes and Total Organic Carbon Weight Percent

All sample powder masses were accurately determined (~2 g) and then acidified with 6 N HCl to remove all carbonate minerals. The insoluble residues were then rinsed several times in ultrapure (deionized, 18.2 MΩ) water until a neutral pH was achieved and dried overnight. The residues were homogenized and weighed into tin cups for analysis. The $\delta^{13}C_{org}$ values were obtained using a Costech Elemental Analyzer coupled to a ThermoFinnigan DeltaPlus XP IRMS via open-split Conflo III at the NHMFL at FSU. The weight percent of total organic carbon (TOC) is determined by the comparison of voltages for the ion beam intensities of masses 44, 45,

and 46 for CO_2^+ between the samples and the known weight percent carbon of the gravimetric standard Acetanilide (e.g., Young et al., 2008). Analytical precision of ±0.2‰ for $\delta^{13}C_{org}$ and ±0.7% for %C is based on long-term, replicate analysis of laboratory standards calibrated to IAEA standards.

2.3 Carbonate-Associated Sulfate Sulfur Isotopes

Carbonate-associated sulfate extractions were performed with minor procedural modifications to those outlined by Wotte et al. (2012). Approximately 80 g of sample powder was rinsed three times in 10% NaCl solution and three times in ultrapure water for 12 h per rinse. Then, 6N HCl was titrated into the samples for ≤ 2 h to liberate sulfate from the carbonate matrix. Insoluble residues were separated from the acidified solution via centrifugation, and the remaining solutions were then brought up to a pH of 10 with NaOH. The precipitates from this reaction were removed via vacuum filtration and the remaining solution brought to pH 4 with several drops of 12 M HNO_3. Excess saturated $BaCl_2$ was then added and allowed to precipitate as barite ($BaSO_4$) for up to 72 hours. The barite was rinsed several times in ultrapure water and dried before being weighed into tin cups with V_2O_5 for sulfur isotope analysis using a Thermo Isolink Elemental Analyzer coupled to a Thermo Delta V Plus IRMS via Conflo-IV open split interface at the NHMFL at FSU. Sulfur isotope results are reported in standard δ-notation with units reported in ‰ relative to V-CDT (Vienna Cañon Diablo Troilite). Analytical precision based on long-term, replicate analysis of lab standards calibrated to IAEA standards is ±0.2‰ or better (1σ).

2.4 Pyrite Sulfur Isotopes and Pyrite Weight Percent

Chromium reducible sulfides were extracted from 0.5–3.0 g of powder from the Priekule-20 drill core samples using modified protocols from Canfield et al. (1986) and Brüchert and Pratt

(1996). Powders were reacted with a 70:30 mixture of 12 N HCl and 1 M $CrCl_3 \cdot 6H_2O$ in a N_2 purged flask. Evolved H_2S gas was then reacted with $AgNO_3$ to precipitate Ag_2S. The total amount of Ag_2S precipitate was gravimetrically determined to calculate weight percent pyrite, assuming quantitative stoichiometry. Approximately 350 µg of homogenized Ag_2S was weighed into tin cups with V_2O_5 and analyzed for $\delta^{34}S_{pyr}$ values using a Thermo Isolink Elemental Analyzer coupled to a ThermoFisher Delta V Plus IRMS via Conflo-IV interface at the NHMFL at FSU. Sulfur isotope results are reported in standard δ-notation with units reported in ‰ relative to V-CDT (Vienna Cañon Diablo Troilite). Analytical precision based on long-term, replicate analysis of lab standards calibrated to IAEA standards is ±0.2‰ or better (1σ).

2.5 Manganese Concentrations

Bulk elemental composition of the Priekule-20 drill core samples was determined through multi-acid digestion. Sample masses of 50-100 mg of were weighed into teflon beakers and microwave digested using a CEM MARS 6 to remove organic carbon without volatilizing redox-sensitive trace elements. Samples were then digested in a standard multi-step trace metal acid digestion using various combinations of trace-metal clean HNO_3, HCl, and HF. These acids were added to the samples, kept on hotplates (~120-180°C) for 24-48 h, and dried down before having more acid added. Remaining organic matter post-microwaving was oxidized with ultra-pure H_2O_2. After complete dissolution of the samples, they were dried down and dissolved in 2% HNO_3 for analysis on an Agilent 7500cs quadrupole inductively coupled plasma mass spectrometer (ICP-MS) for trace metal concentrations at the NHMFL at FSU. Manganese concentrations are reported with and without carbonate correction to account for variable TIC content. Blank concentrations were below detection limits and replicate analyses of USGS standard SDO-1 were within < 2 % of the reported Mn value. Importantly, this method measures

the total elemental abundance in all mineral phases in a sample. Thus, our [Mn] values do not only reflect Mn-oxides but also other Mn mineral phases in the sediments such as Mn-carbonates or Mn bound to sulfides.

2.6 Thallium Isotopes

Approximately 50-100 mg of powdered sample were treated with 3 mL of 2 M HNO_3 and heated at 130°C for ~12 hours to chemically separate the authigenic thallium (Tl; Owens et al., 2017). This acid treatment dissolves the pyrite in the samples, which is thought to contain the authigenic fraction of Tl (Nielsen et al., 2011). Samples were centrifuged multiple times and the supernatant (authigenic fraction) was separated from the undissolved silicate-bound detrital fraction. The solution was treated with a 50:50 solution of concentrated HNO_3-HCl and left overnight on a hot plate at 120°C. The solution was then reacted with 1 mL of either 50% HNO_3 or HCl and 100 µL high purity H_2O_2 and placed on a hot plate at 130°C for a few hours to remove organic matter (Owens et al., 2017). Samples were then prepared for anion exchange chromatography to separate Tl from the sample matrix, particularly lead (Pb), using established protocols (Rehkämper and Halliday, 1999; Nielsen et al., 2004). Thallium purification (and quantitative removal of Pb) was accomplished using a single micro-column procedure (Ostrander et al., 2017) with AG1-X8 anion exchange resin.

Samples were then appropriately diluted and spiked with NIST SRM 981 Pb for measurement on a Neptune multi-collector ICP-MS at the NHMFL. Thallium isotope analyses were accomplished using standard-sample bracketing and normalizing to the NIST SRM 981 Pb to monitor for instrumental mass bias (e.g. Rehkämper et al., 2002; Nielsen et al., 2009). Thallium isotope composition is reported relative to NIST SRM 997 Tl standard and reported in epsilon notation:

$$\varepsilon^{205}Tl = ({}^{205}Tl/{}^{203}Tl_{sample} - {}^{205}Tl/{}^{203}Tl_{SRM997}) / ({}^{205}Tl/{}^{203}Tl_{SRM997}) \times 10{,}000 \quad \text{Eq. 1}$$

Error for thallium isotope values are given as 2 standard deviations (σ) based on replicate analyses of each sample. Samples with 2σ values < ±0.3 were plotted and reported with ±0.3 ε unit error bars based on the long-term chemical processing and analytical precision of the USGS shale standard SCo-1. Multiple analyses of SCo-1 were completed simultaneously with our samples and had an average $\varepsilon^{205}Tl$ of -3.17 ± 0.46 (2σ, n=4), which is within the reported value (-3.0 ± 0.3) of other recent work (Owens et al., 2017; Ostrander et al., 2017; Them et al., 2018; Ostrander et al., 2019).

3. Diagenetic Assessment

All sedimentary strata experience some amount of post-depositional processes that have the potential to alter primary geochemical signatures. As a result of recrystallization, carbonate rocks are particularly susceptible to potential alteration processes. It is important to determine if the stable isotope trends from this study reflect a primary seawater signal or are the result of post-burial processes, diagenetic or otherwise (e.g., Banner and Hanson, 1990; Railsback et al., 2003). The covariation observed in cross plots of geochemical proxy data can be used to determine the degree of diagenetic alteration the sediments and/or rocks have experienced since deposition (e.g., Lohmann, 1988; Hurtgen et al., 2002; Cramer and Saltzman, 2005; Swart and Eberli, 2005; Gill et al., 2008; Jones and Fike, 2013).

3.1 Carbon

A linear relationship between $\delta^{13}C_{carb}$ and $\delta^{18}O_{carb}$ can be indicative of the partial resetting of carbon and oxygen isotope values via the influence of meteoric waters (Railsback et al., 2003). A cross plot of our $\delta^{13}C_{carb}$ and $\delta^{18}O_{carb}$ data (Fig. DR3A) indicates no correlation for

either set of data ($R^2 < 0.1$). The $\delta^{13}C_{org}$ values may also be affected by diagenetic alteration through thermal heating or oxidative loss of volatile organic compounds (Meyers, 1994), which is particularly important for more organic matter-rich facies such as those of the deep, basinal Latvian samples. The shallow-water carbonate samples from Gotland show no correlation between $\delta^{13}C_{org}$ and TOC wt% ($R^2 = 0.013$; Fig. DR3C), indicating no apparent thermal alteration. This is supported by Gotland conodont studies that report very low conodont alternation index (CAI) values of ≤ 1 (Jeppsson, 1983). The Latvian samples are moderately correlated ($R^2 = 0.413$) which may be indicative of some amount of thermal alteration from this locality. However, the CAI values for drill cores from this area of Latvia indicate these strata experienced very limited thermal heating (CAI = 1–2; Kaljo et al., 1997).

The $\delta^{13}C_{carb}$ values from each locality were also cross plotted against weight percent of total inorganic carbon (wt. % TIC) to evaluate the possibility of facies changes and sea level impacting the stable isotope trends (Fig. DR3B). The $\delta^{13}C_{carb}$ data from the Latvia locality are weak-moderately correlated ($R^2 = 0.319$; Fig. DR3B) to wt. % TIC, but this does not necessarily imply that sea level related facies changes are controlling the shifts in carbon isotopes in the Latvia succession or globally. Strong support for the Lau CIE being the result of global biogeochemical carbon cycle perturbation is found in the fact that this CIE has been documented on multiple paleocontinents in a wide variety of shallow water carbonate facies and from deeper water, siliciclastic mudstone/shale facies (e.g., Calner, 2008 and references therein). The $\delta^{13}C_{carb}$ data from the Gotland locality has little to no direct correlation with wt. % TIC ($R^2 = 0.117$; Fig. DR3B) and therefore not related to carbonate facies changes. However, in the Gotland locality the influence of changing sea level can be clearly observed in the lowered $\delta^{13}C_{carb}$ values during the middle of the Lau CIE interval as a clastic delta prograded out into that portion of the Baltic

Basin (Fig. 3A: Burgsvik Sandstone). However, not only does fluctuating sea level play a part in any local depositional conditions but also the local redox conditions, amongst other variables (e.g. sedimentation rates, sediment sources, etc.). Thus, correlations between $\delta^{13}C_{carb}$ and wt % TIC do not preclude the influence of changing redox conditions on each of these variables (e.g., Rose et al., 2019).

3.2 Sulfur

Studies by Gill et al. (2008) and Sim et al. (2015) show that diagenetic processes can lower carbonate-associated sulfate (CAS) concentrations in carbonate rocks, as a result of the flow of sulfate-poor meteoric waters, but have little to no effect on $\delta^{34}S_{CAS}$ values. The cross plots of $\delta^{18}O_{carb}$ vs. [CAS] from the Gotland locality have a moderate correlation ($R^2 = 0.440$; Fig. DR3D). The generally low [CAS] and the moderate correlation with $\delta^{18}O_{carb}$ is likely indicative of minor meteoric diagenetic influence on CAS concentrations (e.g. Gill et al., 2008; Sim et al., 2015). The $\delta^{34}S_{CAS}$ vs. [CAS] ($R^2 = 0.210$; Fig. DR3E) and $\delta^{18}O_{carb}$ vs. $\delta^{34}S_{CAS}$ ($R^2 = 0.106$; Fig. DR3F) cross plots both had weak correlation indicating $\delta^{34}S_{CAS}$ values have not been considerably altered during diagenesis. Therefore, trends in our $\delta^{34}S_{CAS}$ values are largely representative of ancient seawater, with only limited influences by meteoric or burial processes.

Another possible concern for the preservation of the primary geochemical signals of $\delta^{34}S_{CAS}$ in the Gotland locality is the incorporation of contaminant sulfate into the carbonate-associated sulfate. This can be caused by the oxidation of reactive, syn-depositional pyrite during diagenesis or chemical extraction upon exposure to acidic conditions, which can result in lowered $\delta^{34}S_{CAS}$ values (Marenco et al., 2008; Wotte et al., 2012). Specific care was taken during drill core and field sampling to avoid horizons with visible pyrite or iron oxide staining. Regardless of the minimal pyrite present at the Gotland locality, care was taken during sample

processing for the CAS extraction to avoid the oxidation of sulfides during the extraction process (see section 2.3 above).

We have cross-plotted the sulfur isotope data from each locality against wt. % TIC to assess the possibility of facies-dependent trends in the data. The $\delta^{34}S_{pyr}$ data from the Latvia locality showed no correlation with wt. % TIC ($R^2 = 0.110$; Fig. DR3H). This indicates that $\delta^{34}S_{pyr}$ trends are likely not facies-dependent. This is unsurprising, as the apparent stratigraphic correlation between the shift from shale to marl in the Latvian locality and the +45‰ excursion in pyrite sulfur is actually offset by ~5 m, with the lithologic transition preceding the sulfur isotope excursion. The $\delta^{34}S_{CAS}$ data from the Gotland locality showed no correlation with facies transitions ($R^2 = 0.064$; Fig. DR3G). It is possible that the plateau (as opposed to a continuation of the rising limb) in the $\delta^{34}S_{CAS}$ data associated with the Burgsvik Sandstone is the result of the influx of riverine sulfate (~ +8‰; e.g. Gill et al., 2011) mixing with marine sulfate in this deltaic environment, similarly to the $\delta^{13}C_{carb}$ trends discussed above.

Sulfate concentrations in the late Silurian oceans were low, ≤ 5-10 mM, relative to the modern seawater concentrations of 28 mM (Gill et al., 2007). Short-term (~ 1 Myr), large-magnitude excursions in sulfur isotopes such as the excursions in $\delta^{34}S_{CAS}$ and $\delta^{34}S_{pyr}$ recorded in the late Silurian Baltic Basin are only feasible during times in Earth history when the oceanic sulfate pool is relatively low as the residence time for sulfate in the oceans would have been much shorter than today (e.g. Gill et al., 2011). Previously published records of $\delta^{34}S_{CAS}$ through the Silurian report a range of values from +21.5 to +35.6‰, with only 32 total data points (e.g. Kampschulte and Strauss, 2004). It is unlikely, however, that such a coarsely-resolved dataset has captured the entire range of possible $\delta^{34}S_{CAS}$ values for the Silurian, let alone for relatively

short-term events such as the sulfur isotope excursion associated with the Lau CIE. Additionally, Gill et al. (2007) report $\delta^{34}S_{CAS}$ values as low as +10.9‰ for latest Silurian (Pridoli Stage) strata.

4. Manganese and Thallium Geochemistry

Total manganese concentrations [Mn] were measured in the distal, Latvian locality to provide a local redox context for the Tl isotope measurements. As establishing the timing of geochemical and biotic perturbations is critical to our understanding of the LKE and Lau CIE, the use of [Mn] as a local redox proxy is particularly useful for its rapid response to local changes in oxygen conditions. Having a high redox potential, oxidized Mn (III/IV) is rapidly reduced to Mn^{2+} as oxygen concentrations decrease in dysoxic to anoxic conditions (Rue et al, 1997; Algeo and Maynard, 2004). This results in the dissolution of Mn-oxides under low-oxygen conditions, the recycling of soluble Mn^{2+} in the water column, and the possible deposition of other types of Mn-minerals (e.g., sulfides, carbonates; Force and Cannon, 1988; Force and Maynard, 1991; Dickens and Owen, 1994; Algeo and Maynard, 2004; Owens et al., 2017). An expansion of anoxia over previously oxygenated sediment can lead to the dissolution of the existing Mn-oxides (e.g. Algeo and Maynard, 2004) and coupled with decreased oxide burial this will lead to an increase in the seawater Mn inventory. In stratified anoxic basins, significant amounts of non-oxide Mn minerals, such as Mn-carbonates, can be buried as a “bathtub ring” along the chemocline where there is mixing of anoxic waters with overlying oxic waters that are well mixed with the atmosphere, as is seen in the modern day Black Sea (Force and Cannon, 1988; Force and Maynard, 1991; DeLange et al., 2008). Total sedimentary Mn concentrations enriched above average crustal values of 850 ppm (Calvert and Pedersen, 1993; Morford and

Emerson, 1999; Turgeon and Brumsack, 2006; Boyer et al., 2011) likely represent more oxidizing conditions which bury Mn-oxides.

The global burial flux of Mn-oxides exerts a strong control on the seawater Tl isotope value. A large isotopic fractionation occurs during the adsorption of Tl onto Mn-oxides (+12 and +18 epsilon unit difference between seawater and Mn-oxide Tl; as reviewed in Nielsen et al., 2017). Thus, in order to capture seawater using organic-rich sediments, it is imperative to avoid the local incorporation of Mn-oxides due to the large fractionation. The reported range in the Tl isotope values of Mn-oxides is due to the analysis of hydrogenetic and diagenetic ferromanganese crusts, which also includes oxic clay minerals. The average Mn-oxide fractionation is ~ +16 epsilon units and there are currently no data that suggest this has varied systematically or due to environmental perturbations, including direct biological controls. If there was Tl isotope contamination from local Mn-oxides, there should be a relationship between [Mn] and Tl isotopes such that samples with elevated [Mn] would have a more positive ε^{205}Tl signature due to local Mn-oxide contamination. Our [Mn], however, are generally low and there is only a weak correlation between [Mn] and ε^{205}Tl with an $R^2 = 0.235$ (Fig. DR3I). The carbonate content in the Latvian core ranges from 10-70% with an average of ~31%. Thus, carbonate-corrected [Mn] values are plotted to account for likely dilution of trace metals by variable carbonate deposition (e.g. Lyons et al., 2009; Owens et al., 2016). The trends in the uncorrected and carbonate corrected [Mn] data are very similar, but the influence of carbonate dilution is clear in the most carbonate-rich horizons (those with the largest difference in values).

During the peak of the CIE, there is a brief increase in total [Mn] just after the first peak of the Tl isotope excursion (Fig. 2), however, the concentrations remain below the 850 ppm threshold (with the exception of a few carbonate-corrected values). This increase could be related

to local and/or global dynamics. This could be driven by a local increase in Mn-oxide burial or a result of the influence of higher riverine input bringing more oxygen into this part of the Baltic Basin as sea level dropped and rivers prograded into the Baltic Basin, as evidenced by the deposition of the Burgsvik Sandstone in Gotland (compare Fig. 2 and DR2 for data correlation). However, if this [Mn] shift was driven by an increase in *local* Mn-oxides the Tl isotopes should record a similar shift due to the large isotope fractionation associated with Mn-oxides. Another possibility is that a global decrease in Mn-oxide burial flux due to oceanic deoxygenation would likely increase the global dissolved Mn reservoir which could allow for the greater burial of non-oxide Mn minerals, increasing total sedimentary [Mn]. Importantly, Tl isotopes track the burial of Mn-oxides, but do not preclude the burial of other Mn mineral phases. A similar phenomenon has been observed in carbonates during Oceanic Anoxic Event 2 (Jenkyns et al., 2017) which occurs roughly as Tl isotopes shift in black shales (Ostrander et al., 2017).

5. Lau/Kozlowskii Extinction Interval

5.1 Stratigraphic range of the Lau/Kozlowskii Extinction

The placement of the Lau/Kozlowskii Extinction (LKE) intervals in Figures 2 and 3 are meant to provide an easy relative time-orientation when viewing each of these primary geochemical data figures. Each rectangle encompasses the approximate range of both the Lau conodont event (e.g. Jeppsson and Aldridge, 2000; Jeppsson, 2005; Calner, 2008) and the Kozlowskii graptolite event (e.g. Urbanek, 1993; Kaljo et al., 1997; Lehnert et al., 2007; Manda et al., 2012). This is particularly useful as the two events are asynchronous, as discussed in the main text. See above discussion (Section 1) for precise details on correlation of the two localities.

In the Latvia drill core (Fig. 2) the reference point for the LKE is the local last appearance datum (LAD) of *Neocucullograptus kozlowskii* (Kaljo et al., 1997). This has been extended after the *N. kozlowskii* LAD as a gradient to account for the uncertainty that the local LAD represents the global *N. kozlowskii* LAD as there are no graptolites present at all through a portion of this drill core. The LKE interval has been expanded prior to the *N. kozlowskii* LAD and into the *Bohemograptus bohemicus tenuis* Zone to account for the earlier timing of the beginning of Lau conodont extinction event. This correlation with the Lau event based on the co-occurrence of conodonts and graptolites in the interbedded shale and carbonate strata of Vidukle drill core, Latvia and Bohemia terrane sections (Kaljo and Martma, 2006; Lehnert et al., 2007; Manda et al., 2012). The presence of a gradient at the lower end of the interval reflects the minor uncertainty in correlation of particular biozones between sections (Gotland to Latvia) and across paleocontinents (e.g., Bohemia to Baltica).

In Gotland, the Lau event is defined by the practical last appearance datum (pLAD) of *Polygnathoides siluricus*, where the abundance of *P. siluricus* decreases substantially, at the base of the Botvide Member of the När Formation (Jeppsson, 2005; Eriksson and Calner, 2008). The Botvide Member is not present as a set of marker beds in the Uddvide-1 drill core (Fig. 3). As a result of this set of carbonate facies not being present in the studied drill core, we placed the lower end of the LKE interval a few meters below the contact between the När and Eke formations, with gradation to show the uncertainty in where the Botvide Member should be correlated to from other nearby drill cores and outcrops on Gotland (see Eriksson and Calner, 2008 for further detail). The upper boundary of the LKE on this figure extends to the top of the *Icriodontid* Zone. This was a time of extremely low faunal diversity amongst conodonts, which Jeppsson (e.g., 2005) considered to be a part of the Lau event interval. This also correlates with

the later Kozlowskii graptolite extinction event, the color gradient at the top of this interval signifies the minor degree of uncertainty in that correlation.

We emphasize again that the LKE is highly asynchronous (e.g. Munnecke et al., 2003; Stricanne et al., 2006; Lehnert et al., 2007; Manda et al., 2012). It is important to note that while the LKE interval as it is presented here captures the extinction interval of many of the fauna affected, such as conodonts (e.g. Jeppsson, 2005), graptolites (e.g. Manda et al., 2012), fish (Eriksson et al., 2009), and brachiopods (e.g. Boucot et al., 1975), there are exceptions. The LKE interval as we have described it does not encompass the acritarch extinction which, as noted in the main text, occurs notably later than the other extinctions (Stricanne et al., 2006).

5.2 Expanded Details for Integration of Ludfordian Biotic Records with Geochemical Records

Though globally recognized, the mid-Ludfordian LKE has been most thoroughly studied in the Baltic Basin, particularly on Gotland (e.g. Kaljo et al., 1997; Jeppsson, 2005; Stricanne et al., 2006; Eriksson and Calner, 2008; Eriksson et al., 2009). The Ludfordian only has two published absolute ages from U-Pb dating of ash beds in Podolia, Ukraine (Cramer et al., 2015), which are useful for constraining the duration of the Lau CIE (Fig. 4). Conveniently, in all cases where the extinction event has been well-studied a corresponding carbon isotope record has been documented from the same samples or nearby sections (e.g., Calner, 2005; Kaljo et al., 1997; Kaljo and Martma, 2006; Stricanne et al., 2006; Manda et al., 2012).

The biotic data are presented as a percent change in diversity due to a lack in consistency in taxonomic classification available. For example, the graptolite (Manda et al., 2012); conodont (Jeppsson, 2005; Calner, 2008); and fish (Eriksson et al., 2009) data were all available at a species level; whereas the brachiopod data (Boucot, 1975; Talent et al., 1993) were only

available at a genus level. The percent change in diversity was calculated with the pre-extinction interval number of species or genera considered to be 100% with changes deviating from that number. The acritarch data (Stricanne et al., 2006) are only available as abundance data rather than taxonomic diversity, as the study focused on relative changes in several taxonomic groups. Thus, we present it as percent change in abundance but the calculations behind it are otherwise the same.

Due to the variable data sources and focus of these previous studies, some of the biotic records overlap more completely with our geochemical records than others. In Fig. 4A, solid lines represent well constrained (time and diversity) biotic records, and dashed lines represent intervals where the biotic records are not as well-documented, or detailed stage-slice level data is simply not available. Much of the biotic data are from Gotland, including the conodont (Jeppsson, 2005; Jeppsson et al., 2007), fish (Eriksson et al., 2009), and acritarch (Stricanne et al., 2006) records. Abundance and/or diversity trends from these taxonomic groups are well-placed within the context of each other and Ludfordian carbon isotope records as all of these records were generated from either: i) the same samples, ii) the same outcrops/formations, and/or iii) nearby localities. Because of this level detail and integration in the previous paleontological, stratigraphic, and carbon isotope studies of Gotland the biotic trends plotted in Fig 4A in stage-slices Lu1 and most of Lu2 are well constrained with each other and our new geochemical records (Fig. 4B,C,D). The upper Gorstian pre-LKE interval is not necessarily as well studied as the extinction itself, therefore we show no changes in the pre-event strata through stage slice Go2 for most taxa due to a lack of data. The graptolite records are well integrated with Ludlow carbon isotope records and are shown as a solid line on Fig. 4A for the entirety of our study interval based upon previous work from the peri-Gondwanan terrane of Bohemia (Lehnert et al., 2007;

Manda et al., 2012; Fryda and Manda, 2013) and Baltica (Urbanek, 1993; Kozłowski and Sobień, 2012; Urbanek et al., 2012). The brachiopod record, while shown as a solid line, is the coarsest resolution of all the datasets available. Boucot (1975) and Talent et al. (1993) note that the brachiopod extinction happens roughly concurrently with the conodont extinction, but this is largely based upon two bins of data with coarser time resolution. The brachiopod data are a compilation from sections all over the world, originally detailed in Boucot (1975) and expanded upon by Talent et al. (1993).

6. Calculations of geochemical offsets between Tl and C isotope records

The stratigraphic relationship between ε^{205}Tl and δ^{13}C data are comparable to previous studies of Mesozoic OAEs (Ostrander et al., 2017; Them et al., 2018), whereby increased anoxia significantly predated the global positive carbon isotope excursion with peak ε^{205}Tl values being coeval with the beginning of the rising limb of the Lau CIE. The offset between the beginning of deoxygenation (ε^{205}Tl record) and the onset of enhanced global carbon burial (δ^{13}C records) can be approximated utilizing new radiometric ages from late Silurian bentonite ashes (Cramer et al., 2015) and assuming linear sedimentation rates throughout the study interval within the Priekule-20 drill core. The Lau CIE is conservatively estimated to be 1.0 ± 0.21 myr in duration (Cramer et al., 2015), though it could be shorter, and it spans ~36 m of the Latvian drill core studied here. The positive excursion in ε^{205}Tl begins ~ 8 m below the onset of the Lau CIE. Given the estimated range of 0.79 – 1.21 myr for the duration of the CIE, global deoxygenation began at least 175 – 270 ky prior to the CIE, which cannot be driven by differences in residence time in DIC (~100 kyr) *and* Tl (~20 kyr) that are geologically short.

References for GSA Data Repository

Algeo, T.J. and Maynard, J.B., 2004, Trace-element behavior and redox facies in core shales of Upper Pennsylvanian Kansas-type cyclothems: Chemical Geology, v. 206, p. 289-318, doi: 10.1016/j.chemgeo.2003.12.009.

Banner, J.L., and Hanson, G.N., 1990, Calculation of simultaneous isotopic and trace element variations during water-rock interaction with applications to carbonate diagenesis: Geochimica et Cosmochimica Acta, v. 54, p. 3123–3137, doi: 10.1016/0016-7037(90)90128-8.

Boucot, A.J., 1975, Evolution and Extinction Rate Controls: Developments in palaeontology and stratigraphy, Amsterdam, Netherlands, Elsevier Scientific Publishing Company, v. 1, 427 p.

Boyer, D.L., Owens, J.D., Lyons, T.W., and Droser, M.L., 2011, Joining forces: Combined biological and geochemical high-resolution palaeo-oxygen history in Devonian epeiric seas: Palaeogeography, Palaeoclimatology, Palaeoecology, v. 306, p. 134-146, doi: 10.1016/j.palaeo.2011.04.012.

Brüchert, V., and Pratt, L.M., 1996, Contemporaneous early diagenetic formation of organic and inorganic sulfur in estuarine sediments from St. Andrew Bay, Florida, USA: Geochimica et Cosmochimica Acta, v. 60, p. 2325-2332.

Calner, M., 2008, Silurian global events — at the tipping point of climate change, *in* Elewa, A.M.T., ed., Mass extinctions: Berlin Heidelberg, Springer-Verlag, p. 21-58.

Calvert, S.E., and Pederson, T.F., 1993, Geochemistry of recent oxic and anoxic sediments: implications for the geological record: Marine Geology, v. 113, p. 67-88.

Canfield, D.E., Raiswell, R., Westrich, J.T., Reaves, C.M., and Berner, R.A., 1986, The use of chromium reduction in the analysis of reduced inorganic sulfur in sediments and shales: Chemical Geology, v. 54, p. 149-155.

Corradini, C., Corriga, M.G., Männik, P., and Schönlaub, H.P., 2015, Revised conodont stratigraphy of the Cellon section (Silurian, Carnic Alps): Lethaia, v. 48, p. 56-71, doi: 10.1111/let.12087.

Cramer, B.D., and Saltzman, M.R., 2005, Sequestration of ^{12}C in the deep ocean during the early Wenlock (Silurian) positive carbon isotope excursion: Palaeogeography, Palaeoclimatology, Palaeoecology, v. 219, p. 333-349, doi: 10.1016/j.palaeo.2005.01.009.

Cramer, B.D., Schmitz, M.D., Huff, W.D., and Bergström, S.M., 2015, High-precision U-Pb zircon age constraints on the duration of rapid biogeochemical events during the Ludlow Epoch (Silurian Period): Journal of the Geological Society [London], v. 172, p. 157-160, doi: 10.1144/jgs2014-094.

DeLange, G.J., Thomson, J., Reitz, A., Slomp, C.P., Principato, M.S., Erba, E., and Corselli, C., 2008, Synchronous basin-wide formation and redox-controlled preservation of a Mediterranean sapropel: Nature Geoscience, v. 1, p. 606-610, doi: 10.1038/ngeo283.

Dickens, G.R., and Owen, R.M., 1994, Late Miocene-early Pliocene manganese redirection in the central Indian Ocean: Expansion of the intermediate water oxygen minimum zone: Paleoceanography, v. 9, no. 1, p. 169-181.

Eriksson, M.J., and Calner, M., 2008, A sequence stratigraphical model for the Late Ludfordian (Silurian) of Gotland, Sweden: implications for timing between changes in sea level, palaeoecology, and the global carbon cycle: Facies, v. 54, p. 253-276, doi: 10.1007/s10347-007-0128-y.

Eriksson, M.E., Nilsson, E.K., and Jeppsson, L., 2009, Vertebrate extinctions and reorganizations during the Late Silurian Lau Event: Geology, v. 37, no. 8, p. 739-742, doi: 10.1130/G25709A.1.

Force, E.R., and Cannon, W.F., 1988, Depositional model for shallow-marine manganese deposits around black shale basins: Economic Geology, v. 83, p. 93-117.

Force, E.R., and Maynard, J.B., 1990, Manganese: Syngenetic deposits on the margins of anoxic basins: Reviews in Economic Geology, v. 5, p. 147-160.

Fryda, J., and Manda, Š., 2013, A long-lasting steady period of isotopically heavy carbon in the late Silurian ocean: evolution of the $\delta^{13}C$ record and its significance for an integrated $\delta^{13}C$, graptolite and conodont stratigraphy: Bulletin of Geosciences, v. 88, no. 2, p. 463-482, doi: 10.3140/bull.geosci.1436.

Gill, B.C., Lyons, T.W., and Frank, T.D., 2008, Behavior of carbonate-associated sulfate during meteoric diagenesis and implications for the sulfur isotope paleoproxy: Geochimica et Cosmochimica Acta, v. 72, p. 4699-4711, doi: 10.1016/j.gca.2008.07.001.

Gill, B.C., Lyons, T.W., and Saltzman, M.R., 2007, Parallel, high-resolution carbon and sulfur isotope records of the evolving Paleozoic marine sulfur reservoir: Palaeogeography, Palaeoclimatology, Palaeoecology, v. 256, p. 156-173, doi: 10.1016/j.palaeo.2007.02.030.

Gill, B.C., Lyons, T.W., Young, S.A., Kump, L.R., Knoll, A.H., and Saltzman, M.R., 2011, Geochemical evidence for widespread euxinia in the Later Cambrian ocean: Nature, v. 469, p. 80-83, doi: 10.1038/nature09700.

Hurtgen, M.T., Arthur, M.A., Suits, N.S., and Kaufman, A.J., 2002, The sulfur isotopic composition of Neoproterozoic seawater sulfate: implications for a snowball Earth?: Earth and Planetary Science Letters, v. 203, p. 413-429, doi: 10.1016/S0012-821X(02)00804-X.

Jenkyns, H.C., Dickson, A.J., Ruhl, M., and van den Boorn, S.H.J.M., 2017, Basalt-seawater interaction, the Plenus Cold Event, enhanced weathering and geochemical change: deconstructing Ocean Anoxic Event 2 (Cenomanian-Turonian, Late Cretaceous): Sedimentology, v. 64, no. 1, p. 16-43, doi: 10.1111/sed.12305.

Jeppsson, L., 1983, Silurian conodont faunas from Gotland: Fossils and Strata, no. 15, p. 121-144.

Jeppsson, L., 2005, Conodont-based revisions of the Late Ludfordian on Gotland, Sweden: Geologiska Föreningen (GFF), v. 127, p. 273-282, doi: 10.1080/11035890501274273.

Jeppsson, L., and Aldridge, R.J., 2000, Ludlow (late Silurian) oceanic episodes and events: Journal of the Geological Society [London], v. 157, p. 1137-1148.

Jeppsson, L., Talent, J.A., Mawson, R., Simpson, A.J., Andrew, A.S., Calner, M., Whitford, D.J., Trotter, J.A., Sandström, O., and Caldon, H.J., 2007, High-resolution Late Silurian correlations between Gotland, Sweden, and the Broken River region, NE Australia: Lithologies, conodonts and isotopes: Palaeogeography, Palaeoclimatology, Palaeoecology, v. 245, p. 115-137, doi: 10.1016/j.palaeo.2006.02.032.

Jones, D.S., and Fike, D.A., 2013, Dynamic sulfur and carbon cycling through the end-Ordovician extinction revealed by paired sulfate-pyrite $\delta^{34}S$: Earth and Planetary Science Letters, v. 363, p. 144-155, doi: 10.1016/j.epsl.2012.12.015.

Johnson, M.E., 2010, Tracking Silurian eustasy: Alignment of empirical evidence or pursuit of deductive reasoning?: Palaeogeography, Palaeoclimatology, Palaeoecology, v. 296, p. 276-284, doi: 10.1016/j.palaeo.2009.11.024.

Kaljo, D., Kiipli, T., and Martma, T., 1997, Carbon isotope event markers through the Wenlock-Pridoli sequence at Ohesaare (Estonia) and Priekule (Latvia): Palaeogeography, Palaeoclimatology, Palaeoecology, v. 132, p. 211-223.

Kaljo, D., and Martma, T., 2006, Application of carbon isotope stratigraphy to dating the Baltic Silurian rocks: Geologiska Föreningen (GFF), v. 128, p. 123-129, doi: 10.1080/11035890601282123.

Kampschulte, A., and Strauss, H., 2004, The sulfur isotopic evolution of Phanerozoic seawater based on the analysis of structurally substituted sulfate in carbonates: Chemical Geology, v. 204, p. 255-286, doi: 10.1016/j.chemgeo.2003.11.013.

Kiipli, T., Kiipli, E., and Kaljo, D., 2010, Silurian sea level variations estimated using SiO_2/Al_2O_3 and K_2O/Al_2O_3 ratios in the Priekule drill core section, Latvia: Bollottino della Società Paleontologica Italiana, v. 41, no. 1, p. 55-63.

Kozłowski, W., and Munnecke, A., 2010, Stable carbon isotope development and sea-level changes during the Late Ludlow (Silurian) of the Łysogóry region (Rzepin section, Holy Cross Mountains, Poland): Facies, v. 56, p. 615-633, doi: 10.1007/s10347-010-0220-6.

Kozłowski, W., and Sobień, K., 2012, Mid-Ludfordian coeval carbon isotopes, natural gamma ray and magnetic susceptibility excursions in Mielnik IG-1 borehole (Eastern Poland)—Dustiness as a possible link between global climate and the Silurian carbon isotope record: Palaeogeography, Palaeoclimatology, Palaeoecology, v. 339-341, p. 74-97, doi: 10.1016/j.palaeo.2012.04.024.

Kump, L.R., Arthur, M.A., Patzowsky, M.E. Gibbs, M.T., Pinkus, D.S., Sheehan, P.M., 1999, A weathering hypothesis for glaciation at high atmospheric pCO_2 during the late Ordovician: Palaeogeography, Palaeoclimatology, Palaeoecology, v. 152, p. 173-187.

Lehnert, O., Fryda, J., Buggisch, W., Munnecke, A., Nützel, A, Križ, J., and Manda, S., 2007, $\delta^{13}C$ records across the late Silurian Lau event: New data from middle palaeo-latitudes of northern peri-Gondwana (Prague Basin, Czech Republic): Palaeogeography, Palaeoclimatology, Palaeoecology, v. 245, p. 227-244, doi: 10.1016/j.palaeo.2006.02.022.

Lohmann, K.C., 1988, Diagenetic systems and their application in studies of paleokarst, *in* James, N.P. and Choquette, P.W., ed., Paleokarst: New York, Springer-Verlag, p. 58-80.

Lyons, T.W., Anbar, A.D., Severmann, S., Scott, C., and Gill, B.C., 2009, Tracking euxinia in the ancient ocean: a multiproxy prospective and Proterozoic case study: Annual Reviews of Earth and Planetary Sciences, v. 37, p. 507-534, doi: 10.1146/annurev.earth.36.031207.124233.

Manda, S., Štorch, P., Slavík, L., Fryda, J., Križ, J., and Tasáryová, A., 2012, The graptolite, conodont and sedimentary record through the late Ludlow Kozlowskii Event (Silurian) in the shale-dominated succession of Bohemia: Geological Magazine, v. 149, no. 3, p. 507-531, doi: 10.1017/S0016756811000847.

Marenco, P.J., Corsetti, F.A., Kauffman, A.J., and Bottjer, D.J., 2008, Environmental and diagenetic variations in carbonate associated sulfate: An investigation of CAS in the Lower Triassic of the western USA: Geochimica et Cosmochimica Acta, v. 72, p. 1570-1582, doi: 10.1016/j.gca.2007.10.033.

McAdams, N.E.B., Cramer, B.D., Bancroft, A.M., Melchin, M.J., Devera, J.A., and Day, J.E., 2019, Integrated $\delta^{13}C_{carb}$, conodont, and graptolite biogeochemistry of the Silurian from the Illinois Basin and stratigraphic revision of the Bainbridge Group: Geological Society of America Bulletin, v. 113, no. 1/2, p. 335-352, doi: 10.1130/B32033.1.

Meyers, P.A., 1994, Preservation of elemental and isotopic source identification of sedimentary organic matter: Chemical Geology, v. 114, p. 289-302, doi: 10.1016/0009-2541(94)90059-0.
Morford, J.L., and Emerson, S., 1999, The geochemistry of redox sensitive trace metals in sediments: Geochimica et Cosmochimica Acta, v. 63, no. 11-12, p. 1735-1750.
Munnecke, A., Samtleben, C., and Bickert, T., 2003, The Ireviken Event in the lower Silurian of Gotland, Sweden – relation to similar Palaeozoic and Proterozoic events: Palaeogeography, Palaeoclimatology, Palaeoecology, v. 195, p. 99-124, doi: 10.1016/S0031-0182(03)00304-3.
Nielsen, S.G., Goff, M., Hesselbo, S.P., Jenkyns, H.C., LaRowe, D.E., and Lee, C.A., 2011, Thallium isotopes in early diagenetic pyrite – A paleoredox proxy?: Geochimica et Cosmichimica Acta, v. 75, p. 6690-6704, doi: 10.1016/j.gca.2011.07.047.
Nielsen, S.G., Mar-Gerrison, S., Gannoun, A., LaRowe, D., Klemm, V., Halliday, A.N., Burton, K.W., and Hein, J.R., 2009, Thallium isotope evidence for a permanent increase in marine organic carbon export in the early Eocene: Earth and Planetary Science Letters, v. 278, p. 297-307, doi: 10.1016/j.epsl.2008.12.010.
Nielsen, S.G., Rehkämper, M., Baker, J., and Halliday, A.N., 2004, The precise and accurate determination of thallium isotope compositions and concentrations for concentrations for water samples by MC-ICPMS: Chemical Geology, v. 204, p. 109-124.
Nielsen, S.G., Rehkämper, M., and Pritulak, J., 2017, Investigation and Application of Thallium Isotope Fractionation: Reviews in Mineralogy & Geochemistry, v. 82, p. 759-798, doi: 10.2138/rmg.2017.82.18.
Ostrander, C.M., Owens, J.D., and Nielsen, S.G., 2017, Constraining the rate of oceanic deoxygenation leading up to a Cretaceous Oceanic Anoxic Event (OAE-2: ~94 Ma), Science Advances, v. 3, e1701020.
Ostrander, C.M., Nielsen, S.G., Owens, J.D., Kendall, B., Gordon, G.W., Romaniello, S.J., and Anbar, A.D., 2019, Fully oxygenated water columns over continental shelves before the Great Oxidation Event: Nature Geoscience, v. 12, p. 186-191, doi: 10.1038/s41561-019-0309-7.
Owens, J.D., Nielsen, S.G., Horner, T.J., Ostrander, C.M., and Peterson, L.C., 2017, Thallium-isotope compositions of euxinic sediments as a proxy for global manganese-oxide burial: Geochimica et Cosmochimica Acta, v. 213, p. 291-307, doi: 10.1016/j.gca.2017.06.041.
Owens, J.D., Reinhard, C.T., Rohrssen, M., Love, G.D., and Lyons, T.W., 2016, Empirical links between trace metal cycling and marine microbial ecology during a large perturbation to Earth's carbon cycle: Earth and Planetary Science Letters, v. 449, p. 407-417, doi: 10.1016/j.epsl.2016.05.046.
Railsback, L.B., Holland, S.M., Hunter, D.M., Jordan, E.M., Diaz, J.R., and Crowe, D.E., 2003, Controls on Geochemical Expression of Subaerial Exposure in Ordovician Limestones from the Nashville Dome, Tennessee, U.S.A.: Journal of Sedimentary Research, v. 73, p. 790–805, doi: 10.1306/020503730790.
Rehkämper, M., Frank, M., Hein, J.R., Porcelli, D., Halliday, A., Ingri, J., and Liebetrau, V., 2002, Thallium isotope variations in seawater and hydrogenetic, diagenetic, and hydrothermal ferromanganese deposits: Earth and Planetary Science Letters, v. 197, p. 65-81.
Rehkämper, M., and Halliday, A.N., 1999, The precise measurement of Tl isotopic compositions by MC-ICPMS: Application to the analysis of geological materials and meteorites: Geochimica et Cosmochimica Acta, v. 63, p. 935-944.

Rose, C.V., Fischer, W.W., Finnegan, S., and Fike, D.A., 2019, Records of carbon and sulfur cycling during the Silurian Ireviken Event in Gotland, Sweden: Geochimica et Cosmochimica Acta, v. 246, p. 299-316, doi: 10.1016/j.gca.2018.11.030.

Rue, E.L., Smith, G.J., Cutter, G.A., and Bruland, K.W., 1997, The response of trace element redox couples to suboxic conditions in the water column: Deep-Sea Research I, v. 44, no. 1, p. 113-134.

Sim, M.S., Ono, S., and Hurtgen, M.T., Sulfur isotope evidence for low and fluctuating sulfate levels in the late Devonian ocean and the potential link with the mass extinction event: Earth and Planetary Science Letters, v. 419, p. 52-62, doi: 10.1016/j.epsl.2015.03.009.

Stricanne, L., Munnecke, A., and Pross, J., 2006, Assessing mechanisms of environmental change: Palynological signals across the Late Ludlow (Silurian) positive isotope excursion ($\delta^{13}C$, $\delta^{18}O$) on Gotland, Sweden: Palaeogeography, Palaeoclimatology, Palaeoecology, v. 230, p. 1-31, doi: 10.1016/j.palaeo.2005.07.003.

Swart, P.K., and Eberli, G., 2005, The nature of the $\delta^{13}C$ of periplatform sediments: Implications for stratigraphy and the global carbon cycle: Sedimentary Geology, v. 175, p. 115-129, doi: 10.1016/j.sedgeo.2004.12.029.

Talent, J.A., Mawson, R., Andrew, A.S., Hamilton, P.J., and Whitford, D.J., 1993, Middle Paleozoic extinction events: Faunal and isotopic data: Palaeogeography, Palaeoclimatology, Palaeoecology, v. 104, p. 139-152.

Them II, T.R., Gill, B.C., Caruthers, A.H., Gerhardt, A.M., Gröcke, D.R., Lyons, T.W., Marroquin, S.M., Nielsen, S.G., Trabucho Alexandre, J.P., and Owens, J.D., 2018, Thallium isotopes reveal protracted anoxia during the Toarcian (Early Jurassic) associated with volcanism, carbon burial, and mass extinction: Proceedings of the National Academy of Sciences, p. 1-6, doi: 10.1073/pnas.1803478115.

Turgeon, S., and Brumsack, H.J., 2006, Anoxic vs dysoxic events reflected in sedimentary geochemistry during the Cenomanian-Turonian Boundary Event (Cretaceous) in the Umbria-Marche Basin of central Italy: Chemical Geology, v. 234, p. 321-339, doi: 10.1016/j.chemgeo.2006.05.008.

Wotte, T., Shields-Zhou, G.A., and Strauss, H., 2012, Carbonate-associated sulfate: Experimental comparisons of common extraction methods and recommendations toward a standard analytical protocol: Chemical Geology, v. 326-327, p. 132-144, doi: 10.1016/j.chemgeo.2012.07.020.

Urbanek, A., 1993, Biotic crises in the history of the upper Silurian graptoloids: a paleobiological model: Historical Biology, v. 7, p. 29-50.

Younes, H., Calner, M., and Lehnert, O., 2017, The first continuous $\delta^{13}C$ record across the Late Silurian Lau Event on Gotland, Sweden: Geologiska Föreningen (GFF), v. 139, no. 1, p. 63-69, doi: 10.1080/11035897.2016.1227362.

Young, S.A., Saltzman, M.R., Bergström, S.M., Leslie., S.A., and Xu, C., 2008, Paired $\delta^{13}C_{carb}$ and $\delta^{13}C_{org}$ records of Upper Ordovician (Sandbian-Katian) carbonates in North America and China: Implications for paleoceanographic change: Palaeogeography, Palaeoclimatology, Palaeoecology, v. 270, p. 166-178, doi: 10.1016/j.palaeo.2008.09.006.

Supplemental Tables (separate file: 2019342_Tables DR1-DR2.xlsx)

Table DR1: Isotope and geochemical proxy data from the Priekule-20 drill core, Latvia. Carb: carbonate; org: organic; TOC: total organic carbon; TIC: total inorganic carbon; pyr: pyrite; Mn: manganese; Tl: thallium; n: number of replicate analyses per sample used in ε^{205}Tl standard deviation calculation; 2σ: error for Tl isotopes reported as two standard deviations based on replicate analyses of each sample.

Table DR2: Isotope and geochemical proxy data from the Uddvide-1 core and associated outcrop samples, Gotland, Sweden. Carb: carbonate; org: organic; TOC: total organic carbon; TIC: total inorganic carbon; CAS: carbonate associated sulfate.

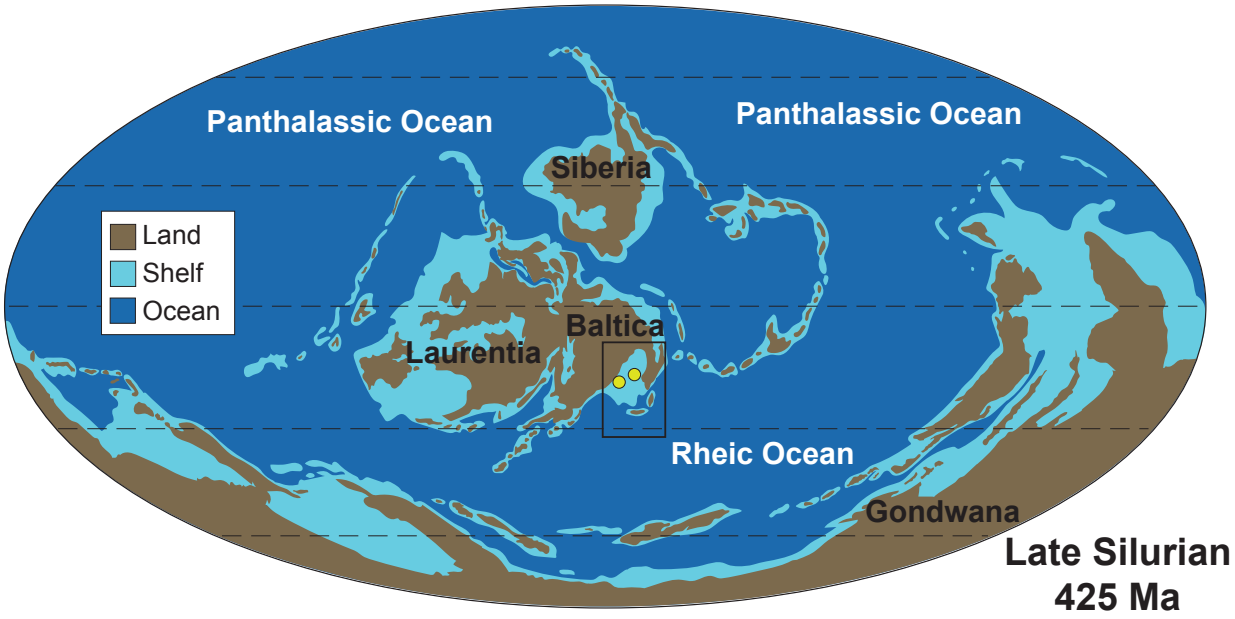

Figure DR1. Global paleogeographic map of the late Silurian, ~425 Ma (after Ron Blakey, https://www2.nau.edu/rcb7/). Area of the Baltic Basin regional map from Fig. 1 is marked by a rectangle. Locations of Swedish Uddvide-1 and Latvian Priekule-20 drill cores are marked by yellow circles.

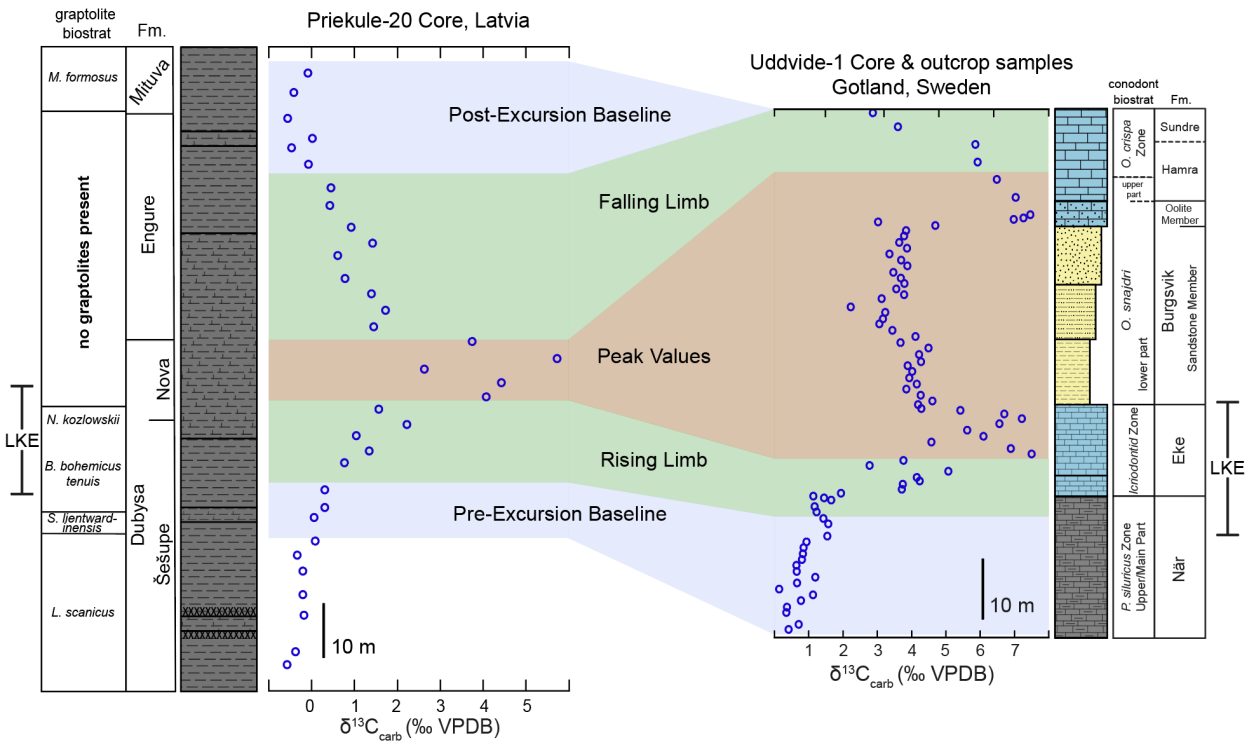

Figure DR2. Correlation between the Latvian Priekule-20 core and the Swedish Uddvide-1 core and related outcrop samples based on graptolite (Kaljo et al., 1997) and conodont (Jeppsson, 2005) biostratigraphy and carbon isotope stratigraphy. Lau/Kozlowskii extinction (LKE) interval bracketed on Latvian and Gotland localities, as it is shown in Fig. 2 & 3 with the yellow bars and defined in supplemental. See supplemental text for further discussion.

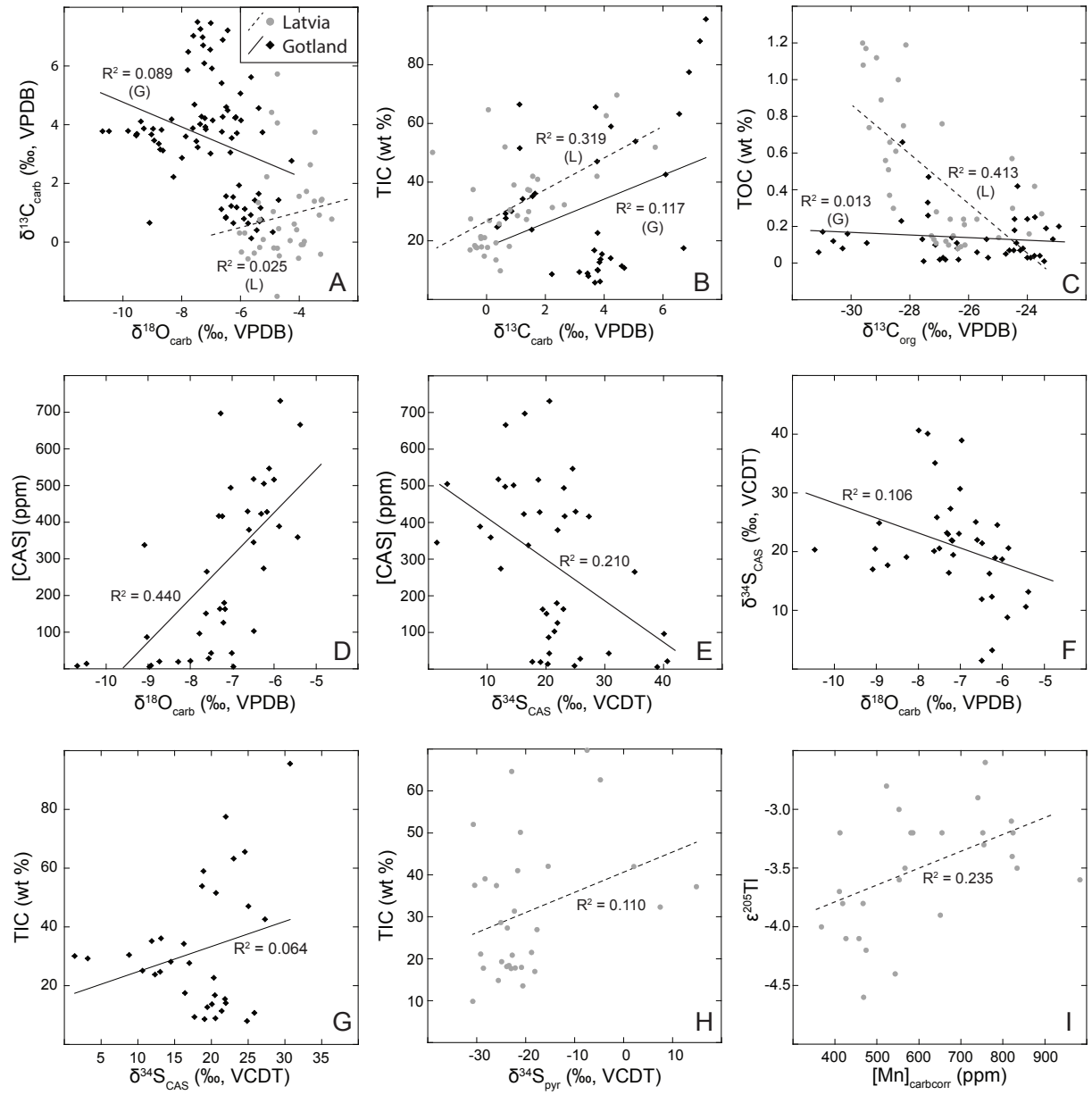

Figure DR3. Cross plots for the evaluation of possible diagenetic alteration of carbon, oxygen, and sulfur isotopes; intra-basinal Mn-oxide deposition on thallium isotopes; pyrite oxidation during CAS extractions; and the possibility of facies dependent carbon and sulfur isotope changes for each locality using total inorganic carbon (TIC) weight percent (wt %) as an indicator of different facies. A: $\delta^{18}O_{carb}$ vs. $\delta^{13}C_{carb}$. B: $\delta^{13}C_{carb}$ vs. wt % TIC. C: $\delta^{13}C_{org}$ vs. wt. % TOC. D: $\delta^{18}O_{carb}$ vs. [CAS]. E: $\delta^{34}S_{CAS}$ vs. [CAS]. F: $\delta^{18}O_{carb}$ vs. $\delta^{34}S_{CAS}$. G: $\delta^{34}S_{CAS}$ vs. wt % TIC. H: $\delta^{34}S_{pyr}$ vs. wt % TIC. I: $[Mn]_{carbcorr}$ vs. $\varepsilon^{205}Tl$.